



ARTICLE

Paraelectric Doping Simultaneously Improves the Field Frequency Adaptability and Dielectric Properties of Ferroelectric Materials: A Phase-Field Study

Zhi Wang¹, Jinming Cao¹, Zhonglei Liu¹ and Yuhong Zhao^{1,2,3,*}

¹School of Materials Science and Engineering, Collaborative Innovation Center of Ministry of Education and Shanxi Province for High-Performance Al/Mg Alloy Materials, North University of China, Taiyuan, 030051, China

²Beijing Advanced Innovation Center for Materials Genome Engineering, University of Science and Technology Beijing, Beijing, 100083, China

³Institute of Materials Intelligent Technology, Liaoning Academy of Materials, Shenyang, 110004, China

*Corresponding Author: Yuhong Zhao. Email: zhaoyuhong@nuc.edu.cn

Received: 19 June 2024 Accepted: 13 September 2024 Published: 15 October 2024

ABSTRACT

Recent years, the polarization response of ferroelectrics has been entirely studied. However, it is found that the polarization may disappear gradually with the continually applied of electric field. In this paper, taking $K_{0.48}Na_{0.52}NbO_3$ (KNN) as an example, it was demonstrated that the residual polarization began to decrease when the electric field frequency increased to a certain extent using a phase-field methods. The results showed that the content of out-of-plane domains increased first and then decreased with the increase of applied electric field frequency, the maximum polarization disappeared at high frequencies, and the hysteresis loop became elliptical. In order to further study the abnormal changes of hysteresis loops of ferroelectrics under high electric field frequency, we analyzed the hysteresis loop and dielectric response of solid solution $0.1SrTiO_3-0.9K_{0.48}Na_{0.52}NbO_3$. It was found that the doped hysteresis loop maintained its shape at higher frequency and the dielectric constant increased. This kind of doping has a higher field frequency adaptability, which has a key guiding role in improving the dielectric properties of ferroelectric thin films and expanding the frequency application range of ferroelectric nano memory.

KEYWORDS

Ferroelectric ceramics; dielectric properties; electric field frequency; doping; phase field method

1 Introduction

Adjusting the domain structure of ferroelectric thin films by varying the electric field frequency holds significant research implications for nano-electronics applications [1,2], including non-volatile memory [3], energy-related devices [4,5], and sensors [6]. Research has demonstrated that the electric field frequency influences the magnitude of the coercive field and the residual polarization [7–9]. Su et al. [10] showed that the frequency-dependent changes in the hysteresis loops of ferroelectric materials result from the direct competition between the velocity of polarization evolution and the velocity of the external load, observing elliptic hysteresis loops at high frequencies. Zhou et al. [11] also found that the residual polarization increases with frequency within a certain range until reaching a



critical value. Zhang et al.'s [12] research indicated that domain structures exhibit higher sensitivity to epitaxial strain at low electric field frequencies, while the polarization vector faces difficulty in achieving a 180° switch at high frequencies due to the rapid alternation of the electric field. These studies collectively demonstrate that the electric field frequency dependence of ferroelectric thin films significantly impacts the domain structure, and the polarization response to the field frequency in most ferroelectric thin films exhibits a critical value. Doping may serve as an effective method to overcome this critical frequency [13].

Studies have shown that when the components of ferroelectric solid solutions vary within a certain range, the dielectric constant is related to the frequency, which also impacts the characteristic parameters of ferroelectric thin films [14]. In other words, chemical modification can affect the residual polarization and coercive force field of thin films [15]. Qi et al. [16] obtained ferroelectric materials with excellent comprehensive properties by using NaNbO₃ doping to refine grains in BiFeO₃-based solid solutions, demonstrating a similarity to the influence of frequency [17]. Therefore, composition changes may affect polarization at different frequencies [18]. K_{0.48}Na_{0.52}NbO₃ (KNN) is a solid solution of the antiferroelectric NaNbO₃ and ferroelectric KNbO₃ [19], which has the potential for high residual polarization [20] and low coercive field, and exhibits good dielectric, electro-mechanical, and piezoelectric properties [21]. Additionally, KNN demonstrates significant polarization changes in the presence of an external electric field [22], and the introduction of SrTiO₃ (STO) may enhance the relaxation behavior of KNN.

This study employs the phase-field method to simulate the domain structure of potassium sodium niobate (KNN) thin films under varying electric field frequencies. The results reveal a non-linear relationship between the out-of-plane domain and frequency, with the domain initially increasing and subsequently decreasing as the frequency changes. Based on these findings, the authors propose a method of doping strontium titanate (STO) to enhance the frequency adaptability of the electric field. The formation of a paraelectric-ferroelectric-antiferroelectric solid solution effectively overcomes the limitations of the original frequency stability while simultaneously improving the dielectric constant. This research provides valuable insights into optimizing the dielectric properties of ferroelectric materials and expanding their applicable frequency range in nano-ferroelectric devices.

2 Method

The phase-field method has emerged as a prominent computational approach for predicting the evolution of nano and mesoscopic microstructures and properties during materials processes [23–26]. It is a computational technique that can calculate, simulate, and predict the spatiotemporal evolution of material microstructure [27–29]. In ferroelectric thin films, the results of domain and domain wall motion can be expressed by polarization [30–32]; thus, the polarization vector $P = (P_1, P_2, P_3)$ is selected as the order parameter. The evolution of spontaneous polarization of ferroelectric thin films over time can be obtained by solving the time-dependent Ginzburg-Landau (TDGL) equation [33].

$$\frac{\partial P_i(\mathbf{r}, t)}{\partial t} = -L \frac{\partial F}{\partial P_i(\mathbf{r}, t)} \quad (1)$$

where \mathbf{r} is the spatial coordinate, t denotes time, L represents the dynamic coefficient, $P_i(\mathbf{r}, t)$ signifies the polarization component at a certain time and position, and F corresponds to the total free energy, which can be expressed as follows:

$$F = \int_V f_{Land}(P_i) + f_{elec}(P_i, E_i) + f_{grad}(P_{i,j}) + f_{elas}(P_i, \varepsilon_{ij}) dV \quad (2)$$

In this expression, f_{Land} , f_{elec} , f_{grad} and f_{elas} represent the Landau energy density, electric field energy density, gradient energy density and elastic energy density, respectively. Additionally, ε_{ij} and E_i denote the components of elastic strain and electric field strength in a specific direction, respectively.

Landau energy is commonly employed to characterize the inherent thermodynamic transformation of a material during a phase transition [34–36]. In the vicinity of the phase transition point, the system's free energy is reduced, and the free energy density can be expanded in the parent phase by applying Landau's theory of second-order phase transitions.

$$\begin{aligned} f_{Land} = & \alpha_1 (P_1^2 + P_2^2 + P_3^2) + \alpha_{11} (P_1^4 + P_2^4 + P_3^4) + \alpha_{12} (P_1^2 P_2^2 + P_2^2 P_3^2 + P_1^2 P_3^2) + \alpha_{123} P_1^2 P_2^2 P_3^2 \\ & + \alpha_{111} (P_1^6 + P_2^6 + P_3^6) + \alpha_{112} (P_1^2 (P_2^4 + P_3^4) + P_2^2 (P_1^4 + P_3^4) + P_3^2 (P_1^4 + P_2^4)) + \alpha_{1111} (P_1^8 + P_2^8 + P_3^8) \\ & + \alpha_{1112} (P_1^6 (P_2^2 + P_3^2) + P_2^6 (P_1^2 + P_3^2) + P_3^6 (P_1^2 + P_2^2)) + \alpha_{1122} (P_1^4 P_2^4 + P_2^4 P_3^4 + P_1^4 P_3^4) \\ & + \alpha_{1123} (P_1^4 P_2^2 P_3^2 + P_2^4 P_3^2 P_1^2 + P_1^4 P_3^2 P_2^2) \end{aligned} \quad (3)$$

The Landau energy coefficient α_1 exhibits a direct relationship with temperature.

The elastic energy density can be expressed as an integral of stress and strain,

$$f_{elas} = \int \sigma_{ij} de_{kl} = \frac{1}{2} c_{ijkl} e_{ij} e_{kl} \quad (4)$$

where c_{ijkl} represents the elastic stiffness tensor, σ_{ij} represents the elastic stress, e_{ij} and e_{kl} represent the elastic strain.

The electrostatic energy density can be expressed as the integral of the electric field and the electric displacement,

$$f_{elec} = - \int E_i dD_i \quad (5)$$

In this formula, $D_i = \varepsilon_0 \varepsilon_r E_j + P_i$. E_i and D_i represent the electric field component and the electric displacement component in the direction i , respectively.

The expression for the gradient energy can be written as follows:

$$f_{grad} = \frac{1}{2} G_{ijkl} P_{ij} P_{kl} \quad (6)$$

where $P_{ij} = \frac{\partial P_i}{\partial x_j}$, and G_{ijkl} is the gradient energy.

In this work, all simulations are performed at $128\Delta x \times 128\Delta y \times 32\Delta z$ discrete grid points, where the actual size $\Delta x = \Delta y = \Delta z = 1$ nm. The thickness of the substrate layer, film layer, and air layer is 10, 20, and 12 nm, respectively. Thicker films exhibit partial relaxation due to mismatch dislocation, which reduces their crystallinity [36]. Considering that material applications generally occur at room temperature, the simulated temperature is set at 298 K. At this temperature, KNN (Potassium Sodium Niobate) thin films possess multi-phase coexisting structures. In this article, frequency is represented by the reciprocal of the time step required for one cycle to simulate the current hysteresis loop (step^{-1}). The time step, a dimensionless quantity, represents the time required for each forward step in the simulation. It is used to discretize the continuous time axis for numerical calculation. The short-circuit boundary condition is employed to eliminate the influence of surface charge and avoid interference from external charge. The relative dielectric constant is set to 45. The KNN parameters used in this simulation were adopted from Reference [22], while the STO (Strontium Titanate) parameters were

obtained from Reference [37]. The simulation is calculated using energy-driven dynamic evolution equations [38], with data derived from experiments or first-principles calculations [39,40]. This work is part of EasyPhase, a phase field software package independently developed by Professor Zhao Yuhong's research group. The ferroelectric phase field module within the software package is utilized. The simulation model and results are incorporated into the EasyPhase software package [41–44].

3 Simulation Results and Analysis

3.1 Evolution of Domain Structure at Different Frequencies

Fig. 1 illustrates the domain direction, where the R phase represents a rhomboid phase with its domain direction pointing out of the plane, the O phase is an orthogonal phase with its domain structure pointing in the plane, and the T phase is a tetragonal phase. The stable domain structure of KNN thin films at various frequencies is depicted in Fig. 2, with different colored areas indicating distinct electrical domains. The specific domain types are denoted on the right. Under a constant applied electric field, the domain structure remains stable without evolution. It is evident that eight types of domains are involved in the switching process, exhibiting a periodic change. Below a frequency of 0.001 step^{-1} , the in-plane domain gradually decreases with increasing frequency, while the opposite trend is observed above this frequency. Fig. 3 presents the polarization vectors at different frequencies, where the direction of the in-plane vector remains nearly constant, and the change in the polarization vector solely involves the variation of the Z-axis polarization component as the electric field frequency increases. Additionally, numerous small-angle domain walls are observed at frequencies below 0.001 step^{-1} , potentially resulting from the brief driving time of electrostatic energy. Similar domain phenomena occur at high frequencies. Before the critical frequency, the in-plane O domain content decreases with increasing frequency, while the out-of-plane R domain content increases. The O domain comprises O_1^+ , O_1^- , O_2^+ , and O_2^- domains, with the corresponding R phase domains being R_1^+ , R_3^+ , R_4^+ , and R_2^+ , respectively. Notably, the variation of these eight domains solely involves the Z-axis polarization component, aligning with the observed changes in the polarization vector diagram. The domain evolution process at high frequencies is the inverse of that at low frequencies. Although the types of domains involved remain consistent, the out-of-plane domain content decreases while the in-plane domain content increases, as shown in Fig. 4. Before a frequency of 0.01 step^{-1} , the content of T_1^+ , T_1^- , T_2^+ , T_2^- , and other domains increases with rising frequency, potentially due to the gradual transformation of the out-of-plane component of the R domain to the in-plane component, resulting in a decrease in the Z-axis component. Above a frequency of 0.02 step^{-1} , the Z-axis component increases due to the reduction of the O domain content, leading to an increase in the out-of-plane component of the R domain. Consequently, the content of the T_3^+ domain, which is a Z-axis component, also increases.

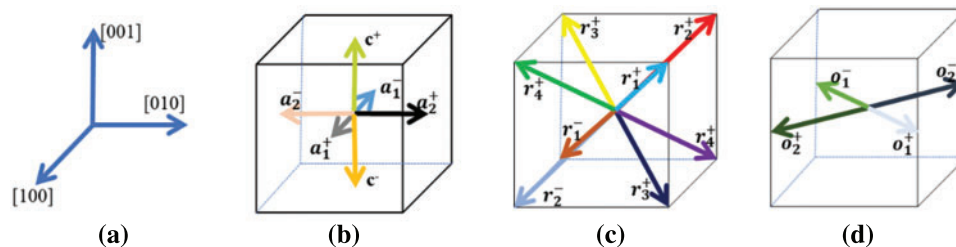


Figure 1: Schematic diagram of different electric domain orientations (a) Axis; polarization component of the (b) T domain (c) R domain (d) Partial O domain

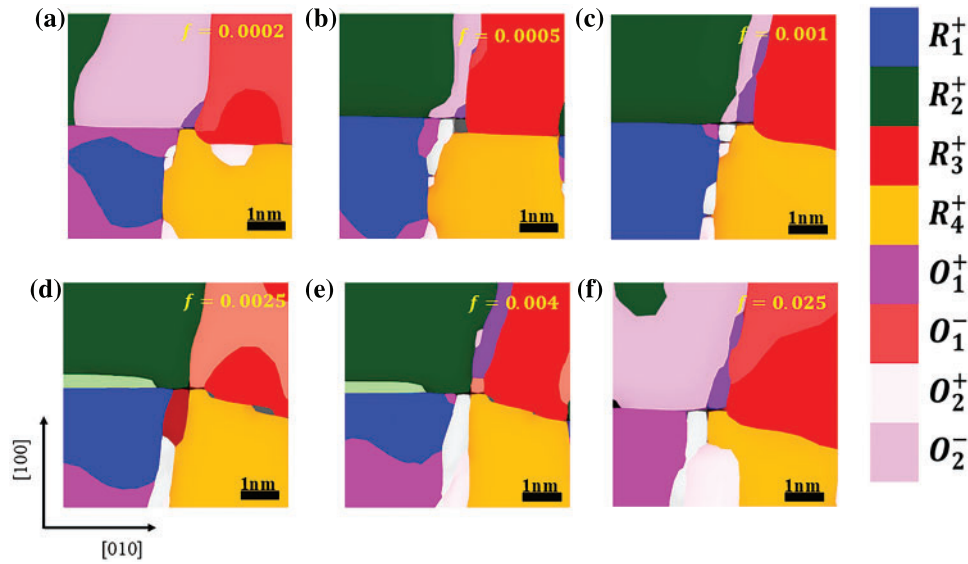


Figure 2: Domain structure of $K_{0.48}Na_{0.52}NbO_3$ thin films in stable state at different frequencies (a) 0.0002 step^{-1} (b) 0.0005 step^{-1} (c) 0.001 step^{-1} (d) 0.0025 step^{-1} (e) 0.004 step^{-1} and (f) 0.025 step^{-1}

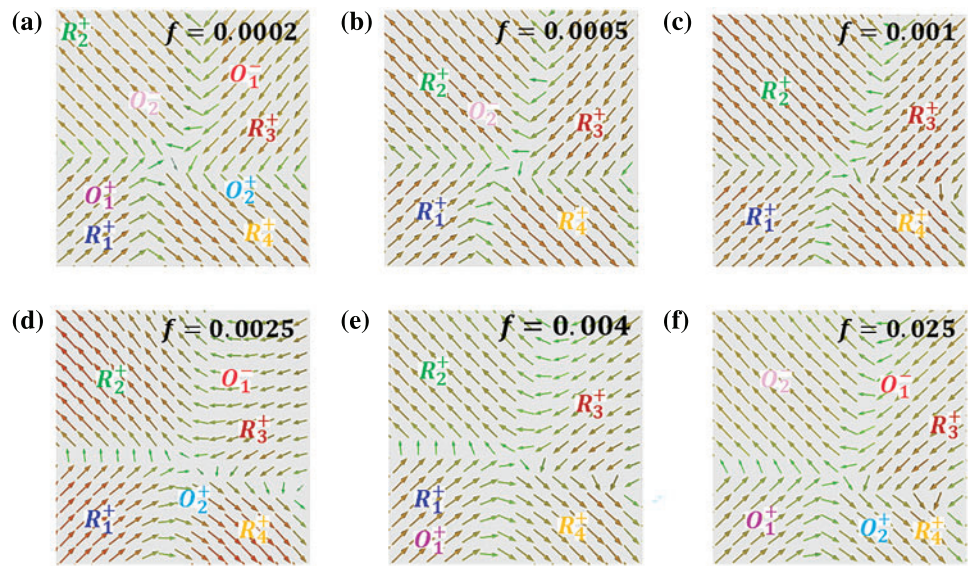


Figure 3: The Polarization vector diagram of $K_{0.48}Na_{0.52}NbO_3$ films is at different frequencies (a) 0.0002 step^{-1} (b) 0.0005 step^{-1} (c) 0.001 step^{-1} (d) 0.0025 step^{-1} (e) 0.004 step^{-1} and (f) 0.025 step^{-1}

In the hysteresis loops of KNN thin films at different frequencies, it is observed that as the frequency increases, the coercive field approaches the applied electric amplitude, as depicted in Fig. 5. The hysteresis loops maintain their normal shape with the frequency change in Fig. 6a–c, while the residual polarization and coercive electric field increase with the rise in frequency, as presented in Table 1. Generally, when the external electric field is applied to the maximum value, the polarization also reaches its peak value, P_{max} . However, starting from Fig. 6d, the maximum polarization value appears at a point lower than the amplitude of the electric field, and subsequently,

the polarization decreases with the increase in the applied electric field. When the electric field frequency surpasses a critical value, the maximum polarization disappears, and the shape of the hysteresis loop gradually transforms into an abnormal elliptical form. As the electric field is gradually unloaded, the polarization increases with the decrease in the electric field, reaching its maximum value at the point of residual polarization. With the increase in the reverse electric field, the coercive field approaches the maximum electric field [45], as illustrated in Fig. 6e. The emergence of the “banana” hysteresis loop may be attributed to a change in the polarization order within the film when the frequency is altered, leading to partial cancellation and resulting in this loss of hysteresis loop. This phenomenon indicates a significant alteration in the material’s properties, rendering it unsuitable for most applications of ferroelectric thin films.

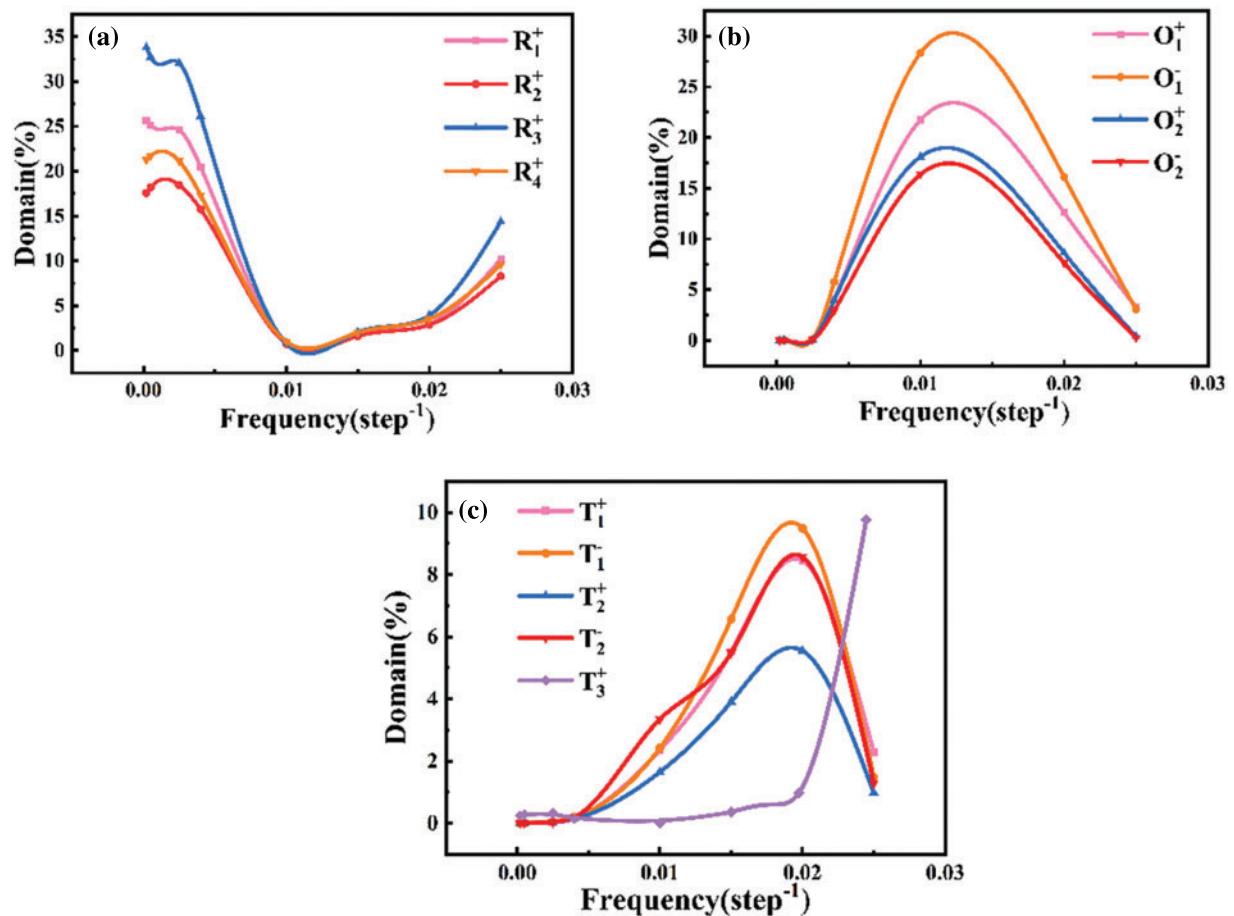


Figure 4: The domain content of KNN thin films changes at different frequencies (a) Variation of R domain content (b) Variation of O domain content (c) Variation of T domain content

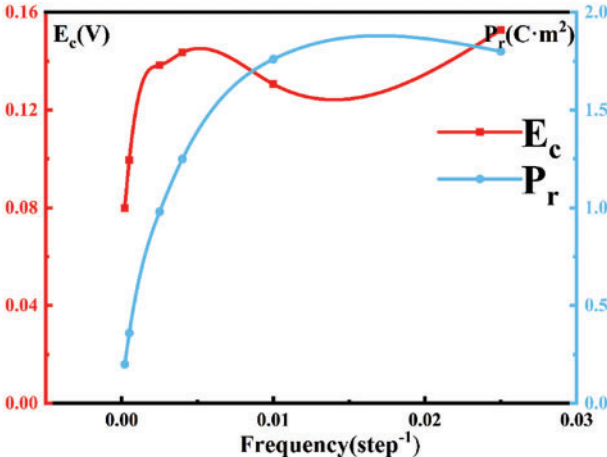


Figure 5: Changes in residual polarization and coercive field of KNN with frequency variation

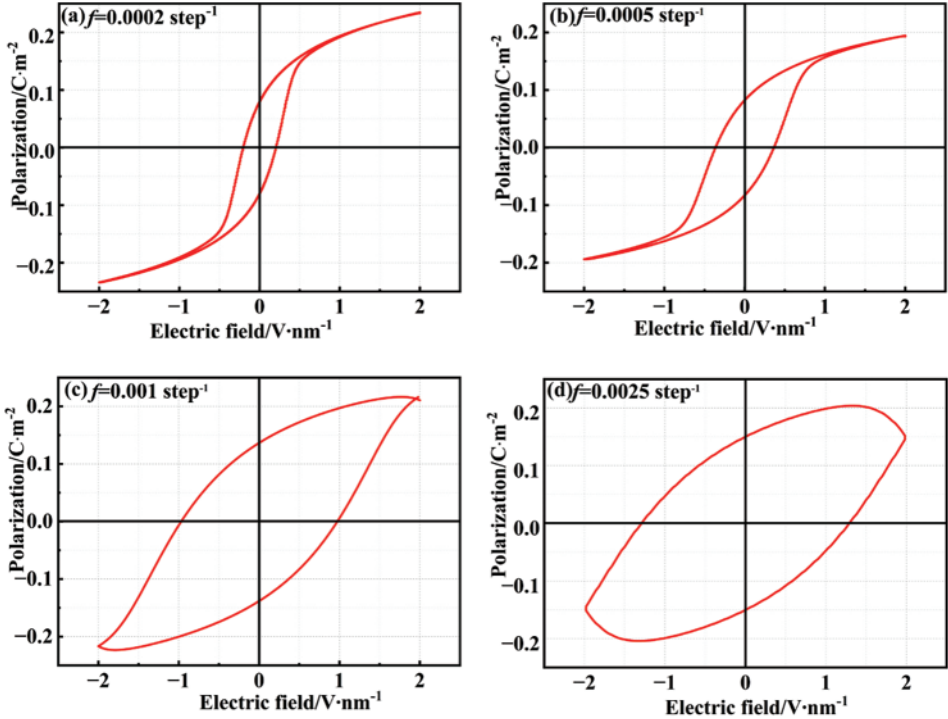


Figure 6: (Continued)

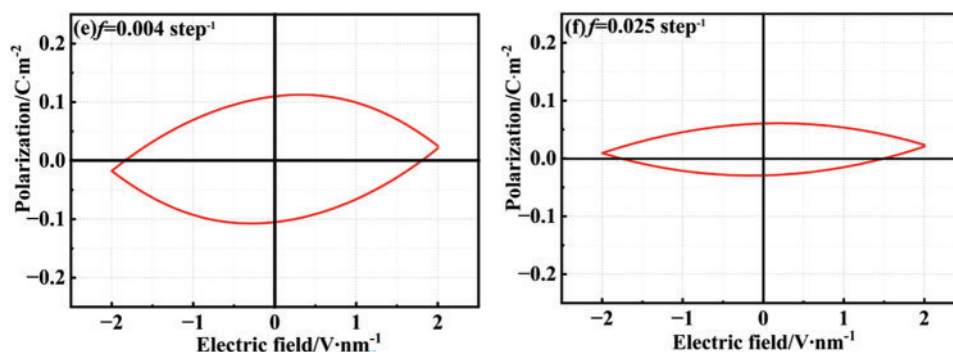


Figure 6: Hysteresis loop of KNN thin film (a) 0.0002 step^{-1} (b) 0.0005 step^{-1} (c) 0.001 step^{-1} (d) 0.0025 step^{-1} (e) 0.004 step^{-1} and (f) 0.025 step^{-1}

3.2 Influence of Frequency of Composition Change on Hysteresis Loops and Dielectric Constants

To further investigate ferroelectrics' polarization response effects under high electric field frequencies, we introduce a paraelectric phase, STO, to the KNN system. The introduction of a paraelectric phase may decrease residual polarization and coercive electric field. Additionally, STO may disrupt long-range ordered ferroelectric dipoles, increase domain wall quantity, and enhance the film's relaxation properties [46]. Experiments have demonstrated that when $x = 0.1$, the solid solution of $(1-x) \text{KNN}-x\text{STO}$ exhibits significant relaxation behavior [14], which may improve frequency stability. Consequently, the components used in the simulation are $0.9\text{K}_{0.48}\text{Na}_{0.52}\text{NbO}_3-0.1\text{SrTiO}_3$. Table 1 presents the residual polarization P_r and coercive force E_c corresponding to pure KNN thin films. The P_r and E_c of doped solid solution thin films near the frequency of 0.001 are significantly smaller than those of pure KNN thin films. When the frequency is 0.0025 step^{-1} and the stable domain structure has evolved, the hysteresis loop of the solid solution thin films does not change significantly, as shown in Fig. 7d. If the field frequency does not exceed this value, the R domain content continues to increase, and the change in residual polarization in the hysteresis loop when the R domain content reaches its maximum does not differ significantly from pure KNN, as shown in Fig. 7a–c. The difference is that the hysteresis loop will not exhibit a shape similar to that in Fig. 6d until the electric field frequency surpasses 0.004 step^{-1} , as shown in Fig. 7e–f. This phenomenon indicates that the introduction of paraelectric STO can effectively delay the formation of an elliptic hysteresis loop. Table 1 reveals that before this frequency, the residual polarization and coercive field of the solid solution material are smaller than those of KNN at the same frequency, improving the material's performance to some extent. The disparate polarization switching processes of these two components at the same frequency may result from grain refinement. The ionic radii of Sr and Ti ions are 0.144 nm and 0.061 nm , respectively, which are smaller than those of K ions (0.164 nm) and Nb ions (0.064 nm), causing lattice distortion [14]. Moreover, comparing the domain structures of the two different components at the same frequency, as shown in Fig. 8, reveals that the content of domains with equal $(1,0,0)$ orientation is significantly reduced in the STO-doped material due to the charge difference between A and B ions in the perovskite material.

Table 1: Residual polarization P_r and coercive field E_c of KNN and 0.9KNN-0.1STO

Frequency	KNN		0.9KNN-0.1STO	
	P_r	E_c	P_r	E_c
0.0002	0.0787	0.20	0.0246	0.08
0.0005	0.0981	0.36	0.0435	0.18
0.001	0.1366	0.96	0.0910	0.60
0.0025	0.1500	1.28	0.1072	0.83
0.004	0.1100	1.84	0.1188	1.44
0.025	0.0606	1.80	0.0613	1.80

4 Discussion

4.1 Domain Changes at Different Frequencies

During the polarization switching process induced by frequency variation, the domain initially tends to switch in the direction of the applied electric field upon its application. As the electric field is removed, the domain gradually switches toward the in-plane orientation. In this reversal process, the electrostatic energy serves as the primary driving force, as illustrated in Fig. 9. It is evident that the energy changes exhibit distinct patterns at the lowest and highest frequencies. At the lowest frequency, the three energy components increase numerically with the increase of the applied electric field, with the electrostatic energy exhibiting the most significant change, indicating its role as the main driving force of domain switching. The electrostatic energy is closely correlated with the applied electric field, resulting in its value following a trend consistent with the applied electric field. At the maximum frequency, the values of elastic energy and Landau energy remain nearly constant, while the electrostatic energy displays a parabolic trend. In this case, the main driving force of domain switching remains the electrostatic energy. However, due to the short duration of electric field application under the high-frequency condition, the electrostatic energy in the high-frequency electric field is considerably smaller compared to that in the low-frequency electric field.

Lower electrostatic energy corresponds to a shorter polarization reversal process, with polarization reversal beginning to recover to its initial state after a brief period. Consequently, the polarization intensity caused by domain switching consistently fluctuates around the applied electric field, as illustrated in Fig. 10. Under low-frequency electric fields, polarization can be completely switched. At 0.001 step^{-1} , the switching time becomes relatively prolonged. In contrast, under high-frequency electric fields, the extent of domain switching is minimal and fails to match the rate of change in the applied electric field. As a result, the Z -axis polarization component of the domain diminishes under high-frequency electric fields, leading to the formation of only a few R domains. This indicates that the content of in-plane domains at residual polarization is substantial.

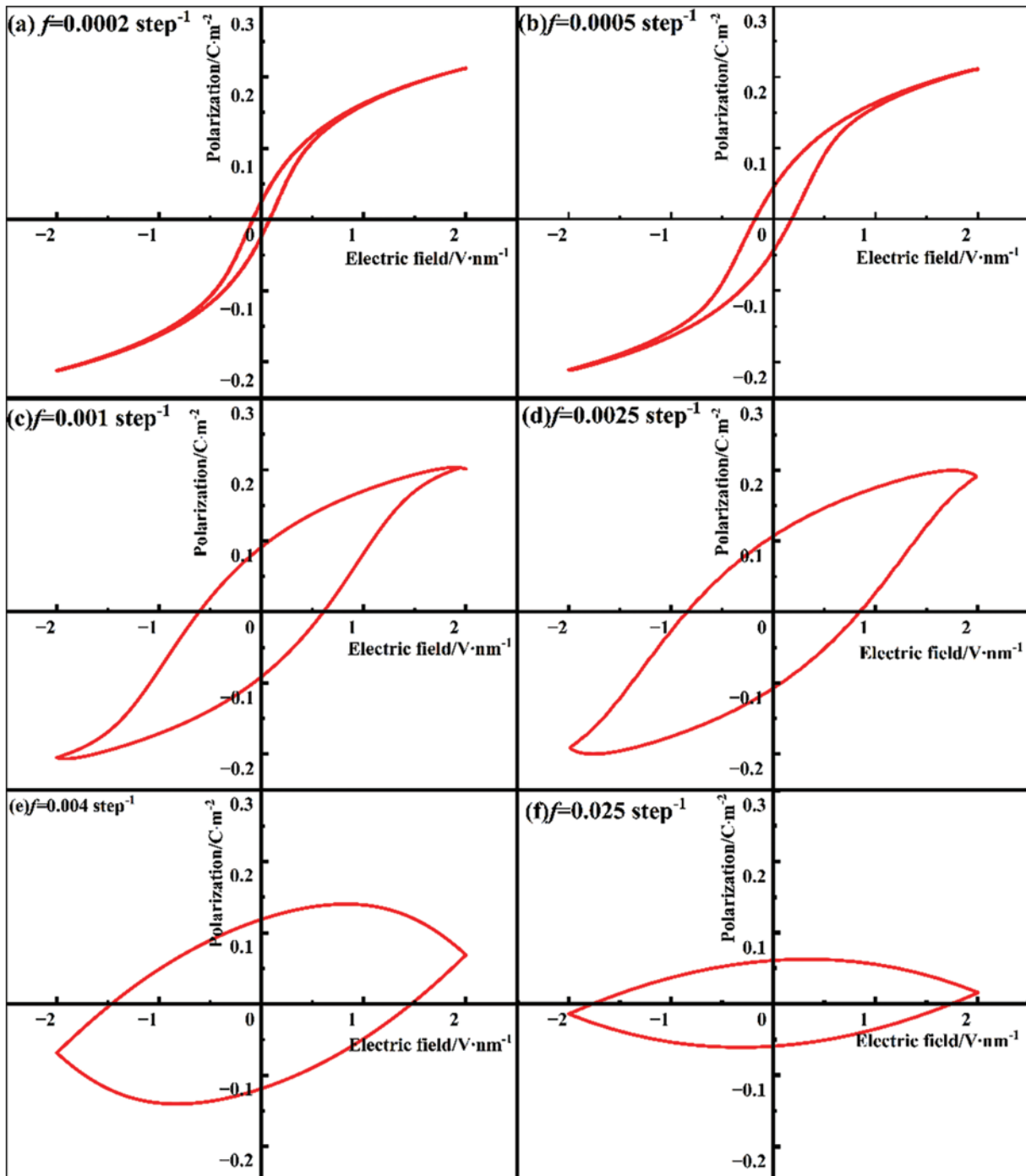


Figure 7: KNN-STO hysteresis loops at different frequencies (a) 0.0002 step^{-1} (b) 0.0005 step^{-1} (c) 0.001 step^{-1} (d) 0.0025 step^{-1} (e) 0.004 step^{-1} and (f) 0.025 step^{-1}

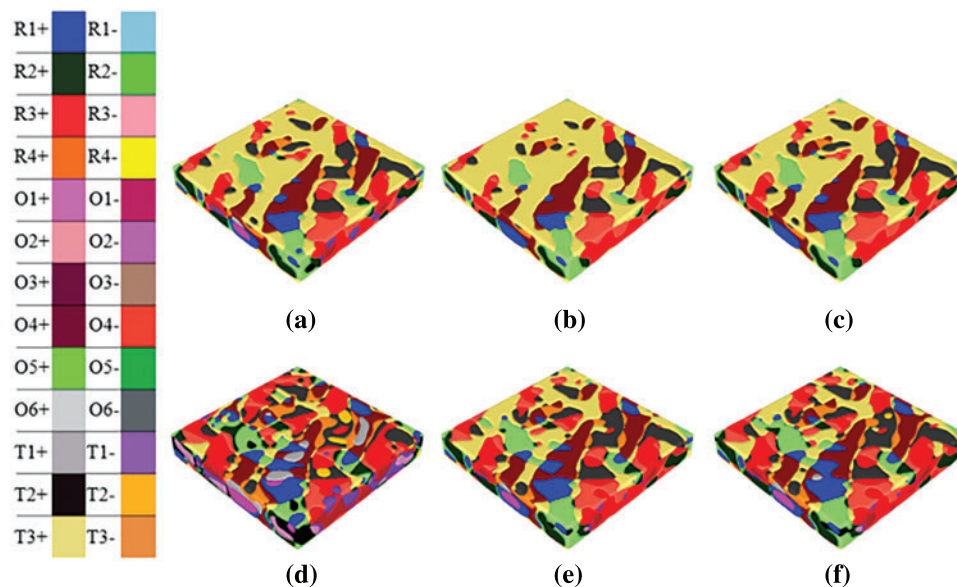


Figure 8: Real-time domain switching behavior at 0.025 step^{-1} : KNN (a) P_{\max} (b) P_r (c) E_c and 0.9KNN-0.1ISTO (d) P_{\max} (e) P_r (f) E_c

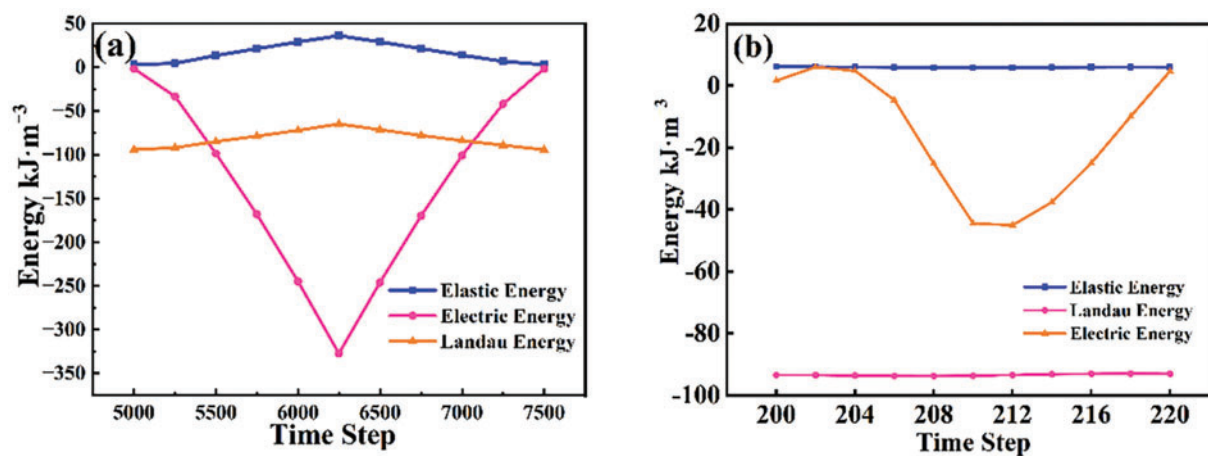


Figure 9: Changes of elastic, electrostatic and landau energies at (a) 0.002 step^{-1} and (b) 0.025 step^{-1} frequencies

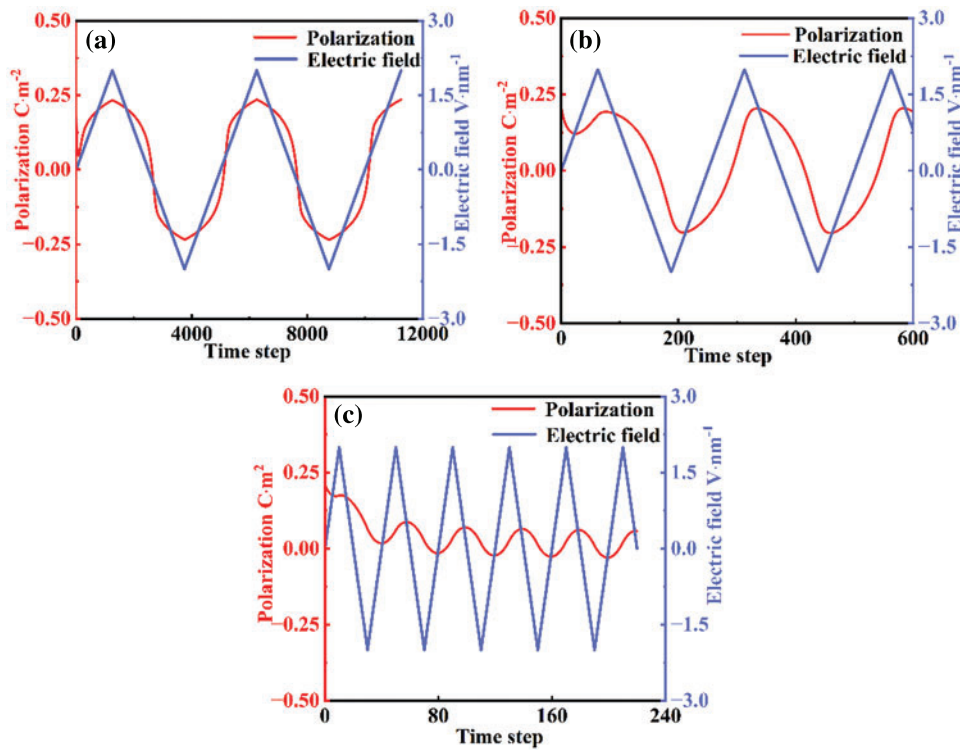


Figure 10: Real-time relationship between polarization switch and applied electric field at frequency of (a) 0.0002 step^{-1} (b) 0.001 step^{-1} (c) 0.025 step^{-1}

4.2 Composition Changes Improve Dielectric Properties of Thin Films

Altering the material composition enhances the film's frequency stability range, as doping or substitution modifies the material's microstructure. The addition of STO may disrupt the long-range ordered ferroelectric dipoles in the KNN-STO solid solution, and the radii of Sr^{2+} and Ti^{4+} ions are relatively small. Lattice distortion caused by substituting K^+ and Nb^{5+} ions in KNN may reduce the film's stability, influencing the material's phase transition [47]. Differences in ionic radii may also induce oxygen vacancies in the lattice, resulting in relaxation behaviors and broadening the film's frequency application range. Fig. 11 illustrates that the material's dielectric constant decreases gradually with increasing frequency, potentially due to the rapid change in electric field direction at high frequencies, whereby the charge lacks sufficient time to respond to the applied electric field changes. At room temperature, in conjunction with the phase diagram, it is evident that domains with the three polarization components (P_1 , P_2 , P_3) exhibit relative stability in KNN thin films without mismatch strain. Fig. 4 demonstrates that the content of domains with the Z-axis component initially decreases and subsequently increases with increasing frequency, exhibiting a minimum value of around 0.01 step^{-1} . The film's stability is compromised near this frequency. Solid solution doping delays the occurrence of the component's minimum frequency, thereby enhancing the film's stability.

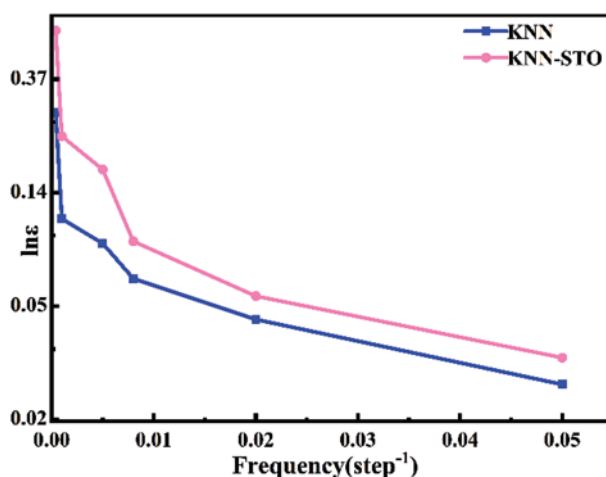


Figure 11: Changes of dielectric constants of KNN and 0.9KNN-0.1STO thin film

5 Conclusion

In this paper, the variation of hysteresis loops under different electric field frequencies was studied through the phase field method. By analyzing the domain content, the difference in the switching mechanism of the KNN domain under different frequencies was clarified. At the residual polarization at lower frequencies, the O-domain content in the plane decreases with the increase of frequency, and the material belongs to the normal application range. When the frequency is greater than 0.001 step^{-1} , the polarization switch is inhibited, and the domain content changes little during the loading field to the unloading field, which makes that the maximum polarization disappears and the residual polarization content decreases, which is very bad for the application of ferroelectric thin films. Based on this, it is proposed to mix STO and KNN in a ratio of 1:9. The addition of STO decreases the domain content of the solid solution (1,0,0) polarization orientation, and increases the domain content in the plane, indicating that the application frequency range of ferroelectric thin films can be expanded by chemical substitution method. Moreover, doping reduces the residual polarization and improves the dielectric properties of the thin films, which provides important guidance for the further expansion of ferroelectric applications.

Acknowledgement: The authors would like to thank the editors and reviewers for their valuable work, as well as the supervisor and family for their valuable support during the research process.

Funding Statement: The work was supported by National Defense Basic Scientific Research Program of China (Grant Nos. JCKY2020408B002, WDZC2022-12).

Author Contributions: Study conception and design: Zhi Wang, Jinming Cao, Zhonglei Liu, Yuhong Zhao; data collection: Zhi Wang, Jinming Cao, Zhonglei Liu; analysis and interpretation of results: Zhi Wang, Jinming Cao, Zhonglei Liu, Yuhong Zhao; draft manuscript preparation: Zhi Wang, Yuhong Zhao. All authors reviewed the results and approved the final version of the manuscript.

Availability of Data and Materials: All the study data are included in the article.

Ethics Approval: Not applicable.

Conflicts of Interest: The authors declare that they have no known competing financial interests or personal relationships that could have appeared to influence the work reported in this paper.

References

- [1] Y. H. Ren, O. Kurt, H. B. Cheng, T. Le, S. Greenbaum and J. Ouyang, “Electrical field driven structural evolutions of polymorphic nanodomains in ferroelectric Ba(Zr,Ti)O₃ films,” *Adv Electron. Mater.*, vol. 8, no. 10, Oct. 2022, Art. no. 2200465. doi: [10.1002/aelm.202200465](https://doi.org/10.1002/aelm.202200465).
- [2] M. H. Tang, G. J. Dong, Y. Sugiyama, and H. Ishiwara, “Frequency-dependent electrical properties in Bi(Zn_{0.5}Ti_{0.5})O₃ doped Pb(Zr_{0.4}Ti_{0.6})O₃ thin film for ferroelectric memory application,” *Semicond Sci. Technol.*, vol. 25, no. 3, Jan. 2010, Art. no. 035006. doi: [10.1088/0268-1242/25/3/035006](https://doi.org/10.1088/0268-1242/25/3/035006).
- [3] K. J. Lee, T. Y. Yang, D. W. Chou, and Y. H. Wang, “Hybrid ferroelectric P (VDF-TrFE)/BZT insulators for pentacene-based nonvolatile memory applications,” *IEEE Electron Device Lett.*, vol. 43, no. 9, pp. 1463–1466, Jul. 2022. doi: [10.1109/LED.2022.3188664](https://doi.org/10.1109/LED.2022.3188664).
- [4] Y. Li *et al.*, “Phase-field simulations of tunable polar topologies in lead-free ferroelectric/paraelectric multilayers with ultrahigh energy-storage performance,” *Adv. Mater.*, vol. 34, no. 13, Apr. 2022, Art. no. 2108772. doi: [10.1002/adma.202108772](https://doi.org/10.1002/adma.202108772).
- [5] J. J. Wang, Y. J. Su, B. Wang, J. Ouyang, Y. H. Ren and L. Q. Chen, “Strain engineering of dischargeable energy density of ferroelectric thin-film capacitors,” *Nano Energ.*, vol. 72, no. 80, Jun. 2020, Art. no. 104665. doi: [10.1016/j.nanoen.2020.104665](https://doi.org/10.1016/j.nanoen.2020.104665).
- [6] W. Shin *et al.*, “Synergistic improvement of sensing performance in ferroelectric transistor gas sensors using remnant polarization,” *Mater. Horiz.*, vol. 9, no. 6, pp. 1623–1630, Apr. 2022. doi: [10.1039/d2mh00340f](https://doi.org/10.1039/d2mh00340f).
- [7] J. N. Wilson, J. M. Frost, S. K. Wallace, and A. Walsh, “Dielectric and ferroic properties of metal halide perovskites,” *APL Mater.*, vol. 7, no. 1, Jan. 2019, Art. no. 010901. doi: [10.1063/1.5079633](https://doi.org/10.1063/1.5079633).
- [8] H. H. Wu, S. G. Cao, J. M. Zhu, and T. Y. Zhang, “The frequency-dependent behavior of a ferroelectric single crystal with dislocation arrays,” *Acta Mech.*, vol. 228, no. 8, pp. 2811–2817, Dec. 2015. doi: [10.1007/s00707-015-1512-2](https://doi.org/10.1007/s00707-015-1512-2).
- [9] X. Chen *et al.*, “Temperature dependence of ferroelectricity and domain switching behavior in Pb(Zr_{0.3}Ti_{0.7})O₃ ferroelectric thin films,” *Ceram. Int.*, vol. 45, no. 14, Oct. 2019, Art. no. 18030. doi: [10.1016/j.ceramint.2019.06.022](https://doi.org/10.1016/j.ceramint.2019.06.022).
- [10] Y. Su, N. Liu, and G. Weng, “A phase field study of frequency dependence and grain-size effects in nanocrystalline ferroelectric polycrystals,” *Acta Mater.*, vol. 87, no. 1, pp. 293–308, Apr. 2015. doi: [10.1016/j.actamat.2015.01.015](https://doi.org/10.1016/j.actamat.2015.01.015).
- [11] G. Z. Zhou *et al.*, “On ferroelectric domain polarization switching mechanism subject to an external electric field by simulations with the phase-field method,” *Sci. China Tech. Sci.*, vol. 56, no. 5, pp. 1129–1138, Feb. 2013. doi: [10.1007/s11431-013-5135-3](https://doi.org/10.1007/s11431-013-5135-3).
- [12] Q. N. Zhang, X. D. Xia, J. Wang, and Y. Su, “Effects of epitaxial strain, film thickness and electric-field frequency on the ferroelectric behavior of BaTiO₃ nano films,” *Int. J. Solids Struct.*, vol. 144–145, no. 6, pp. 32–45, Jul. 2018. doi: [10.1016/j.ijsolstr.2018.04.012](https://doi.org/10.1016/j.ijsolstr.2018.04.012).
- [13] C. H. Jang, H. S. Kim, H. Kim, and H. Y. Cha, “Temperature-and frequency-dependent ferroelectric characteristics of metal-ferroelectric-metal capacitors with atomic-layer-deposited undoped HfO₂ films,” *Materials*, vol. 15, no. 6, Feb. 2022, Art. no. 2097. doi: [10.3390/ma15062097](https://doi.org/10.3390/ma15062097).
- [14] A. Kupec and B. Malič, “Structural and dielectric properties of the lead-free (1–x)K_{0.5}Na_{0.5}NbO₃–xSrTiO₃ thin films from solutions,” *Alloys Compd.*, vol. 596, no. 25, pp. 32–38, May 2014. doi: [10.1016/j.jallcom.2014.01.193](https://doi.org/10.1016/j.jallcom.2014.01.193).
- [15] Y. H. Zhao *et al.*, “Development of phase-field modeling in materials science in China: A review,” *Acta Metall. Sin. (Engl. Lett.)*, vol. 36, no. 11, pp. 1749–1775, Aug. 2023. doi: [10.1007/s40195-023-01593-w](https://doi.org/10.1007/s40195-023-01593-w).
- [16] H. Qi and R. Z. Zuo, “Linear-like lead-free relaxor antiferroelectric (Bi_{0.5}Na_{0.5})TiO₃–NaNbO₃ with giant energy-storage density/efficiency and super stability against temperature and frequency,” *J. Mater. Chem.*, vol. 7, no. 8, Jan. 2019, Art. no. 3971. doi: [10.1039/c8ta12232f](https://doi.org/10.1039/c8ta12232f).

- [17] Y. P. Guo, K. Kakimoto, and H. Ohsato, "Dielectric and piezoelectric properties of lead-free $(\text{Na}_{0.5}\text{K}_{0.5})\text{NbO}_3\text{-SrTiO}_3$ ceramics," *Solid State Commun.*, vol. 129, no. 5, pp. 279–284, Feb. 2004. doi: [10.1016/j.ssc.2003.10.026](https://doi.org/10.1016/j.ssc.2003.10.026).
- [18] H. Pan *et al.*, "Giant energy density and high efficiency achieved in bismuth ferrite-based film capacitors via domain engineering," *Nat. Commun.*, vol. 9, no. 1, May 2018, Art. no. 1813. doi: [10.1038/s41467-018-04189-6](https://doi.org/10.1038/s41467-018-04189-6).
- [19] X. Y. Zhao, J. J. Wang, and L. Q. Chen, "A thermodynamic study of phase transitions and electrocaloric properties of $\text{K}_{0.5}\text{Na}_{0.5}\text{NbO}_3$ single crystals," *Appl. Phys. Lett.*, vol. 116, no. 9, Mar. 2020, Art. no. 092902. doi: [10.1063/1.5144056](https://doi.org/10.1063/1.5144056).
- [20] J. Barr and S. Beckman, "Electrocaloric response of KNbO_3 from a first-principles effective Hamiltonian," *Mater Sci. Eng. B*, vol. 196, pp. 40–43, Jun. 2015. doi: [10.1016/j.mseb.2015.02.004](https://doi.org/10.1016/j.mseb.2015.02.004).
- [21] R. Kumar, A. Kumar, and S. Singh, "Large electrocaloric response and energy storage study in environmentally friendly $(1-x)\text{K}_{0.5}\text{Na}_{0.5}\text{NbO}_3\text{-xLaNbO}_3$ nanocrystalline ceramics," *Sustain. Energ. Fuels*, vol. 2, no. 12, pp. 2698–2704, Sep. 2018. doi: [10.1039/c8se00276b](https://doi.org/10.1039/c8se00276b).
- [22] M. J. Zhou, J. J. Wang, L. Q. Chen, and C. W. Nan, "Strain, temperature, and electric-field effects on the phase transition and piezoelectric responses of $\text{K}_{0.5}\text{Na}_{0.5}\text{NbO}_3$ thin films," *J. Appl. Phys.*, vol. 123, no. 15, Apr. 2018, Art. no. 154106. doi: [10.1063/1.5027505](https://doi.org/10.1063/1.5027505).
- [23] T. Xin *et al.*, "Phase transformations in an ultralight BCC Mg alloy during anisothermal aging," *Acta Mater.*, vol. 239, no. 15, Oct. 2022, Art. no. 118248. doi: [10.1016/j.actamat.2022.118248](https://doi.org/10.1016/j.actamat.2022.118248).
- [24] W. W. Kuang, H. F. Wang, X. Li, J. B. Zhang, Q. Zhou and Y. H. Zhao, "Application of the thermodynamic extremal principle to diffusion-controlled phase transformations in Fe-C-X alloys: Modeling and applications," *Acta Mater.*, vol. 159, no. 15, pp. 16–30, Oct. 2018. doi: [10.1016/j.actamat.2018.08.008](https://doi.org/10.1016/j.actamat.2018.08.008).
- [25] X. L. Tian, Y. H. Zhao, Y. L. Guo, F. Q. Xu, and H. Hou, "Cooperative effect of strength and ductility processed by thermomechanical treatment for Cu-Al-Ni alloy," *Mater Sci. Eng.*, vol. 849, no. 1, Aug. 2022, Art. no. 143485. doi: [10.1016/j.msea.2022.143485](https://doi.org/10.1016/j.msea.2022.143485).
- [26] T. Xin *et al.*, "Ultrahigh specific strength in a magnesium alloy strengthened by spinodal decomposition," *Sci. Adv. Vol.*, vol. 7, no. 23, pp. 1–9, Jun. 2021. doi: [10.1126/sciadv.abf3039](https://doi.org/10.1126/sciadv.abf3039).
- [27] Z. L. Liu, "Topological vortex structure and conductance information storage in ferroelectric ceramics were investigated via phase field method," M.S. thesis, North Univ. of China, Taiyuan, China, 2023.
- [28] Z. L. Liu, J. M. Cao, Z. Wang, and Y. H. Zhao, "Phase-field method explored ferroelectric vortex topology structure and morphotropic phase boundaries," *Acta Phys. Sin.*, vol. 72, no. 3, Feb. 2023, Art. no. 037702. doi: [10.7498/aps.72.20221898](https://doi.org/10.7498/aps.72.20221898).
- [29] L. Q. Chen and Y. H. Zhao, "From classical thermodynamics to phase-field method," *Prog. Mater. Sci.*, vol. 124, no. 2, Feb. 2022, Art. no. 100868. doi: [10.1016/j.pmatsci.2021.100868](https://doi.org/10.1016/j.pmatsci.2021.100868).
- [30] W. L. Zhong, *Ferroelectric physics*. Beijing, China: Science Press, 2000.
- [31] H. Cheng *et al.*, "Demonstration of ultra-high recyclable energy densities in domain-engineered ferroelectric films," *Nat. Commun.*, vol. 8, no. 1, Dec. 2017, Art. no. 1999. doi: [10.1038/s41467-017-02040-y](https://doi.org/10.1038/s41467-017-02040-y).
- [32] T. Sluka, A. K. Tagantsev, D. Damjanovic, M. Gureev, and N. Setter, "Enhanced electromechanical response of ferroelectrics due to charged domain walls," *Nat. Commun.*, vol. 3, no. 1, Mar. 2012, Art. no. 748. doi: [10.1038/ncomms1751](https://doi.org/10.1038/ncomms1751).
- [33] B. Wang, H. N. Chen, J. J. Wang, and L. Q. Chen, "Ferroelectric domain structures and temperature-misfit strain phase diagrams of $\text{K}_{1-x}\text{Na}_x\text{NbO}_3$ thin films: A phase-field study," *Appl. Phys. Lett.*, vol. 115, no. 9, Aug. 2019, Art. no. 092902. doi: [10.1063/1.5116910](https://doi.org/10.1063/1.5116910).
- [34] J. B. Zhang *et al.*, "Rapid solidification of non-stoichiometric intermetallic compounds: Modeling and experimental verification," *Acta Mater.*, vol. 148, no. 115, pp. 86–99, Apr. 2018. doi: [10.1016/j.actamat.2018.01.040](https://doi.org/10.1016/j.actamat.2018.01.040).
- [35] Y. H. Zhao, K. Liu, H. Hou, and L. Q. Chen, "Role of interfacial energy anisotropy in dendrite orientation in Al-Zn alloys: A phase field study," *Mater. Des.*, vol. 216, no. 9, Apr. 2022, Art. no. 110555. doi: [10.1016/j.matdes.2022.110555](https://doi.org/10.1016/j.matdes.2022.110555).

- [36] S. Pradhan, M. Rath, A. David, D. Kumar, W. Prellier and M. R. Rao, "Thickness-dependent domain relaxation dynamics study in epitaxial $K_{0.5}Na_{0.5}NbO_3$ ferroelectric thin films," *ACS Appl. Mater. Interfaces*, vol. 13, no. 30, pp. 36407–36415, Jul. 2021. doi: [10.1021/acsami.1c05699](https://doi.org/10.1021/acsami.1c05699).
- [37] K. M. Rabe *et al.*, *Physics of Ferroelectrics: A Modern Perspective*. Heidelberg, Berlin, Germany: Springer Science & Business Media, 2007.
- [38] T. Yang and L. Q. Chen, "Dynamical phase-field model of coupled electronic and structural processes," *NPJ Comput. Mater.*, vol. 8, no. 1, Jun. 2022, Art. no. 130. doi: [10.1038/s41524-022-00820-9](https://doi.org/10.1038/s41524-022-00820-9).
- [39] H. Pohlmann, J. J. Wang, B. Wang, and L. Q. Chen, "A thermodynamic potential and the temperature-composition phase diagram for single-crystalline $K_{1-x}Na_xNbO_3$ ($0 \leq x \leq 0.5$)," *Appl. Phys. Lett.*, vol. 110, no. 10, Mar. 2017, Art. no. 102906. doi: [10.1063/1.4978360](https://doi.org/10.1063/1.4978360).
- [40] Y. H. Zhao, "Editorial: Phase field method and integrated computing materials engineering," *Front. Mater.*, vol. 10, Feb. 2023, Art. no. 1145833. doi: [10.3389/fmats.2023.1145833](https://doi.org/10.3389/fmats.2023.1145833).
- [41] Y. H. Zhao, B. Zhang, H. Hou, W. Chen, and M. P. Wang, "Phase-field simulation for the evolution of solid/liquid interface front in directional solidification process," *J. Mater. Sci. Technol.*, vol. 35, no. 6, pp. 1044–1052, Jun. 2019. doi: [10.1016/j.jmst.2018.12.009](https://doi.org/10.1016/j.jmst.2018.12.009).
- [42] Y. H. Zhao, "Understanding and design of metallic alloys guided by phase-field simulations," *npj Comput. Mater.*, vol. 9, no. 1, Jun. 2023, Art. no. 94. doi: [10.1038/s41524-023-01038-z](https://doi.org/10.1038/s41524-023-01038-z).
- [43] Y. H. Zhao, T. Z. Xin, S. Tang, H. F. Wang, X. D. Fang and H. Hou, "Applications of unified phase-field methods to designing microstructures and mechanical properties of alloys," *MRS Bull.*, vol. 49, no. 6, pp. 613–625, Jun. 2024. doi: [10.1557/s43577-024-00720-x](https://doi.org/10.1557/s43577-024-00720-x).
- [44] Y. H. Zhao, "Integrated unified phase-field modeling (UPFM)," *MGE Adv.*, vol. 2, no. 2, Jun. 2024, Art. no. e44. doi: [10.1002/mgea.44](https://doi.org/10.1002/mgea.44).
- [45] J. F. Scott, "Ferroelectrics go bananas," *J. Phys.: Condens. Matter*, vol. 20, no. 2, Dec. 2008, Art. no. 021001. doi: [10.1088/0953-8984/20/02/021001](https://doi.org/10.1088/0953-8984/20/02/021001).
- [46] H. Pan *et al.*, "Ultrahigh-energy density lead-free dielectric films via polymorphic nanodomain design," *Science*, vol. 365, no. 6453, pp. 578–582, Aug. 2019. doi: [10.1126/science.aaw8109](https://doi.org/10.1126/science.aaw8109).
- [47] C. W. Bing *et al.*, "Flexible lead-free film capacitor based on $BiMg_{0.5}Ti_{0.5}O_3$ - $SrTiO_3$ for high-performance energy storage," *Chem. Eng. J.*, vol. 445, no. 1, Oct. 2022, Art. no. 136728. doi: [10.1016/j.cej.2022.136728](https://doi.org/10.1016/j.cej.2022.136728).